Optical and magneto-optical properties of highly distorted Fe(100) thin films

J. L. Menéndez,* G. Armelles, and A. Cebollada

Instituto de Microelectrónica de Madrid (Centro Nacional de Microelcatrónica Consejo Superior de Investigaciones Cientficas),
Issac Newton 8-PTM-28760 Tres Cantos, Madrid, Spain

D. Weller

IBM Almaden Research Center, 650 Harry Rd., San Jose, California 95120

Anna Delin

Fritz-Haber-Institut der Max-Planck-Gesellschaft Faradayweg 4-6, 14195 Berlin, Germany
(Received 30 March 2000; revised manuscript received 2 June 2000)

TiN-capped epitaxial bcc Fe films exhibit strong changes in the out-of-plane interplanar distance depending on the growth conditions. At room temperature, the increase of the volume per Fe atom appears to be as large as 5%. The observed distortions deviate substantially from elastic behavior. We explain this effect as due to the presence of nitrogen incorporated into the Fe film during the capping layer deposition. In order to elucidate the effect that these distortions might have on the optical and magneto-optical properties, we study the diagonal and off-diagonal elements of the conductivity tensor for both distorted and undistorted structures. This is done by means of spectral ellipsometry and the Kerr effect in polar and transverse configurations in the energy range from 1.5 to 4.5 eV. Theoretical calculations using *ab initio* techniques for the observed structures are performed and compared with experimental data. Different possible mechanisms for the experimentally observed effects such as distortion, grain size, and orbital hybridization are studied and discussed.

I. INTRODUCTION

The strain in thin films is well known to have an important influence on many different kinds of physical properties. To mention a few examples, it can modify the growth modes of thin films,[1,2] the critical temperature in superconductors,[3] or the optical properties of semiconductors[4] and metals.[5] Regarding magnetic properties, strain also affects saturation magnetoresistance,[6] magnetic permeability,[7] saturation magnetostriction,[8] and magnetic anisotropies.[9] Nevertheless, and despite its basic and technological relevance, little work has been done on the influence that strain can have on the magneto-optical properties of materials.[10,11]

Typically, the experimentally measured magneto-optical magnitudes are the polar complex Kerr effect (θ_k and ϵ_k) or the transverse Kerr signal ($\Delta r/r$). With the surface normal in the z direction, the polar Kerr effect is related to σ_{xy}, while the transverse Kerr signal is related to σ_{xz} or σ_{yz}. A tetragonal distortion of the crystal structure is expected to modify the elements of the conductivity tensor, both the diagonal and off-diagonal ones, since the electronic structure is altered. In particular, a tetragonal distortion along the z direction might break the equivalence between σ_{xy}, σ_{xz}, and σ_{yz} that holds in a cubic system. Taking bcc Fe as a model system, very well studied from both experimental[12–16] and theoretical[17–21] points of view, we will focus on the determination and study of the diagonal and off-diagonal elements of the conductivity tensor for highly tetragonally distorted Fe thin films and compare them with the properties of relaxed Fe.

This paper has the following structure. In Sec. II we describe the different experimental and theoretical techniques used. Section III is devoted to the study and modification of strain in thin Fe films. In Sec. IV we describe and interpret the results obtained from the optical and magneto-optical characterizations and compare them with band-structure-based theoretical calculations. Finally, both the origin of the strain and its possible effects on the magneto-optical spectra will be discussed in Sec. V, followed by conclusions in Sec. VI.

II. EXPERIMENT AND THEORETICAL CALCULATIONS

200 Å bcc Fe films were epitaxially grown on MgO(100) substrates by triode sputtering in an UHV system. The growth temperature of the Fe films was varied from room temperature (RT) up to 700 °C in steps of 100 °C, while the Ar pressure was kept at 4×10^{-4} mbar. In order to protect the Fe films from oxidation, a 15 Å TiN capping layer was reactively sputtered at RT in the same deposition system. The composition of the mixture of gases was 70% Ar and 30% N_2, and the total pressure during deposition of TiN was 8×10^{-4} mbar.

The structure was studied *in situ* by reflection high-energy electron diffraction (RHEED), and *ex situ* by x-ray diffraction (XRD) to obtain the lattice parameters and x-ray reflectometry (XRR) to obtain the thicknesses of the films, using a four-circle diffractometer. Optical constants (n and k) were studied by spectral ellipsometry in the energy range 1.5–4.5 eV. Magneto-optical constants were determined by combined polar and transverse Kerr spectroscopy, in the energy ranges 0.8–5.3 and 1.5–4.5 eV, respectively.

The theoretical spectra presented here were calculated within density functional theory[22] using the local density approximation[23] to the density functional, combined with a full-potential linear muffin-tin orbital basis set.[24] Our present calculations are very similar to the ones published in Ref. 11.
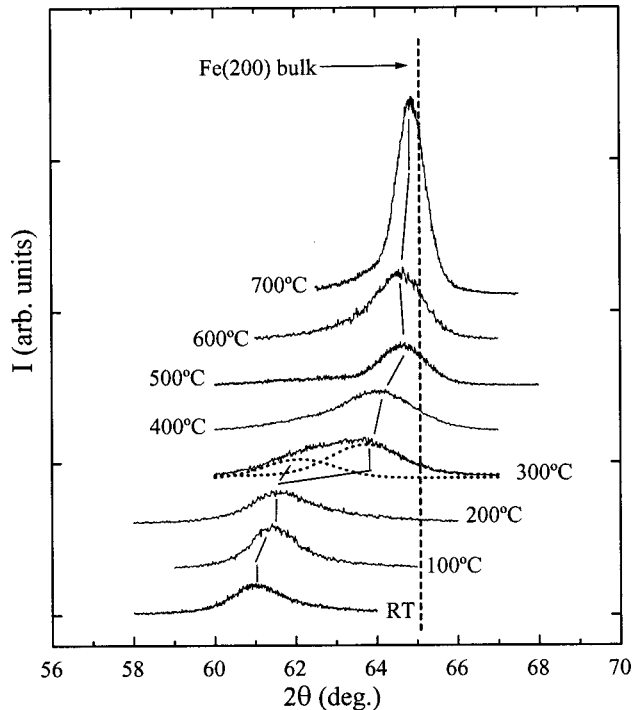
PRB <u>62</u> 10 498

FIG. 1. High-angle XRD symmetric scans showing the displacement of the Fe(200) peak as a function of temperature for samples grown at different temperatures. The dotted line shows the position for bulk Fe(200). The need for two Gaussian peaks to fit the peak at 300 °C indicates the presence of two coexisting phases with high and low degrees of distortion.

In order to account for the indirect intraband transitions, which give a strong contribution at low energies to the diagonal components of the conductivity tensor for metals, we added a phenomenological Drude term $\sigma_D = \omega_P^2/4\pi(\gamma_D - i\omega)$, where ω is the photon frequency, ω_P the unscreened plasma frequency, and γ_D the inverse relaxation time. We used the experimental values 4.9 eV for ω_P and 0.45 eV for γ_D.

III. GROWTH-TEMPERATURE-DEPENDENT LATTICE DISTORTION

Epitaxy was checked through RHEED and XRD analysis. Intense and sharp lines were observed in RHEED patterns for the sample grown at 700 °C, indicative of a high crystalline quality. Samples grown at lower temperatures exhibited similar RHEED patterns, but with broader lines, indicating also good crystalline quality, although less perfect than in the sample grown at 700 °C. Figure 1 shows symmetric XRD scans from the series of Fe samples grown in the range RT to 700 °C, all of them with the TiN capping layer mentioned. A strong displacement in the position of the Fe(200) diffraction peaks is observed as a function of growth temperature, which indicates a growth-temperature-dependent expansion of the out-of-plane lattice parameter. Both in-plane and out-of-plane lattice parameters were determined from the positions of the Fe(200) symmetric and the (110), (211), and (112) asymmetric diffraction peaks. Contrary to what one would expect considering an elastic deformation of the Fe lattice, the in-plane Fe interplanar distances are close to the bulk

TABLE I. In- and out-of-plane lattice parameters and corresponding out-of-plane expansion for Fe films grown at different temperatures.

Growth temp (°C)	In-plane lattice parameter (Å)	Out-of-plane lattice parameter (Å)	Out-of-plane expansion (%)
50	2.86	3.034	5.8
100	2.866	3.016	5.2
200	2.864	3.006	4.9
300	2.863	2.989–2.921	4.3–1.9
400	2.868	2.913	1.6
500	2.873	2.884	0.6
600	2.873	2.889	0.8
700	2.874	2.875	0.3

values within experimental error. For the out-of-plane interplanar spacings, two different regimes of vertical expansion can be clearly distinguished from Fig. 1. The samples grown at RT, 100, and 200 °C are highly distorted, with a vertical expansion between 5% and 6% compared to bulk values, while samples grown at 400 °C and above are much more relaxed, with a vertical distortion between 1.6% and 0.3%. The sample grown at 300 °C shows two diffraction peaks close to each other, which we attribute to the coexistence of two phases in the same film with different lattice parameters, representing the boundary between the low-growth-temperature regime (LGT samples) and the high-growth-temperature regime (HGT samples). Experimental values for the out-of-plane and in-plane lattice parameters of the different Fe films are presented in Table I. It is important to keep in mind that XRD structural characterization was performed *ex situ*, after the growth of the TiN layer.

IV. OPTICAL AND MAGNETO-OPTICAL CONSTANTS FOR DISTORTED Fe

In Fig. 2 we present the real (n) and imaginary (k) parts of the complex refractive index of samples grown at 100 and 700 °C, representative of the LGT and HGT regimes respectively. The spectra were deduced from ellipsometry measurements assuming abrupt interfaces and using the experimental values of the refractive index of TiN, obtained from a TiN film grown under identical conditions to the presently used capping layer. As a comparison, values of the refractive index obtained for bulk Fe samples by other authors[12,13] are also presented in Fig. 2. The main difference between the LGT and HGT samples is the increase of the optical absorption with growth temperature, i.e., with decreasing lattice distortion.

In Fig. 3 we present the transverse Kerr spectra of the same two samples for an angle of incidence of 50°. The most important feature observed in both spectra is the peak at around 2 eV, which is much narrower and more intense in the HGT sample. On the other hand, Fig. 4 shows the complex polar Kerr effect of the same samples. No marked differences are found in this case between the 100 and 700 °C samples, except for slightly higher values of ϵ_k for the sample grown at 100 °C.

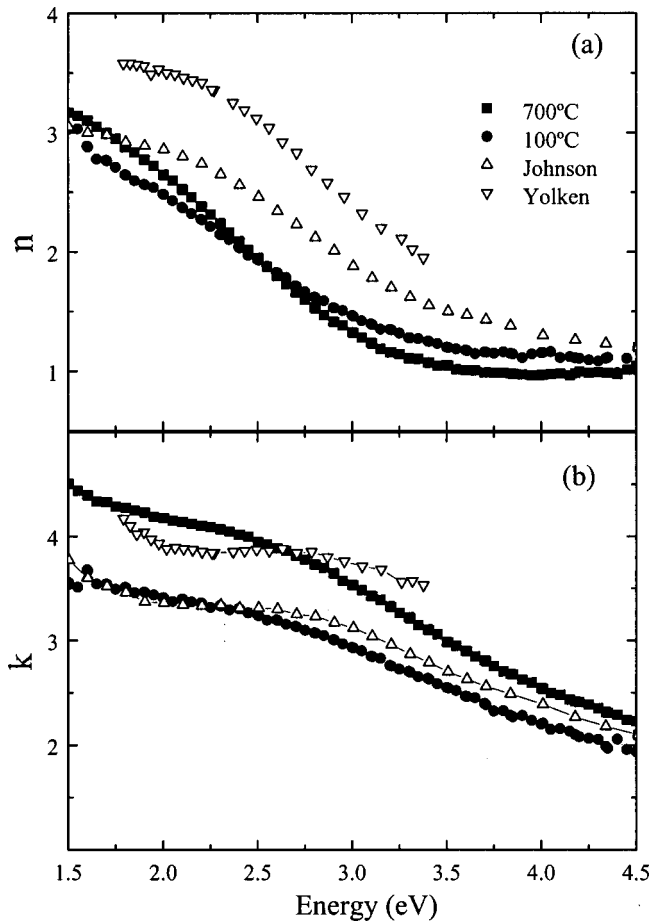A transfer matrix formalism[25,26] was used to calculate the

FIG. 2. Real (a) and imaginary (b) parts of the refractive index for selected samples with high and low degrees of distortion. Up and down triangles are data from other authors (see Refs. 12 and 13).

values of σ_{xy} from the experimentally measured spectra of the refractive indices (n, k) as well as the complex polar Kerr spectra, and the values of σ_{yz} from n and k as well as the transverse Kerr spectra ($\Delta r/r$) obtained at two angles of incidence (50° and 70°). Figures 5 and 6 show, respectively, the real and imaginary parts of the two off-diagonal components σ_{xy} and σ_{yz} of the conductivity tensor for the selected samples, whereas Fig. 7 shows the real and imaginary parts of the diagonal components, extracted from the measured refractive indices. Theoretical curves for $\text{Re}(\sigma_{xy})$, $\text{Im}(\sigma_{xy})$, $\text{Re}(\sigma_{xx})$, and $\text{Im}(\sigma_{xx})$, calculated using experimentally determined in-plane and out-of-plane lattice parameters of the selected samples, are also shown in the same figures, as well as experimental results from other authors.[12–15,27]

Comparing our experimental spectra in Figs. 5(a), 5(b), 6(a), and 6(b), it is evident that the shape of the *xy* and *yz* experimental spectra of the same sample is very similar, but the absolute values are higher in the *yz* component than in the *xy* component. We attribute part of this difference to insufficient magnetic field to saturate the samples in the polar Kerr measurement. Therefore, as the spectral shape is equivalent for σ_{xy} and σ_{yz}, the tetragonal distortion does not induce appreciable difference between these components for a specific distorted sample. Nevertheless, the distortion does produce important differences between the spectra for the
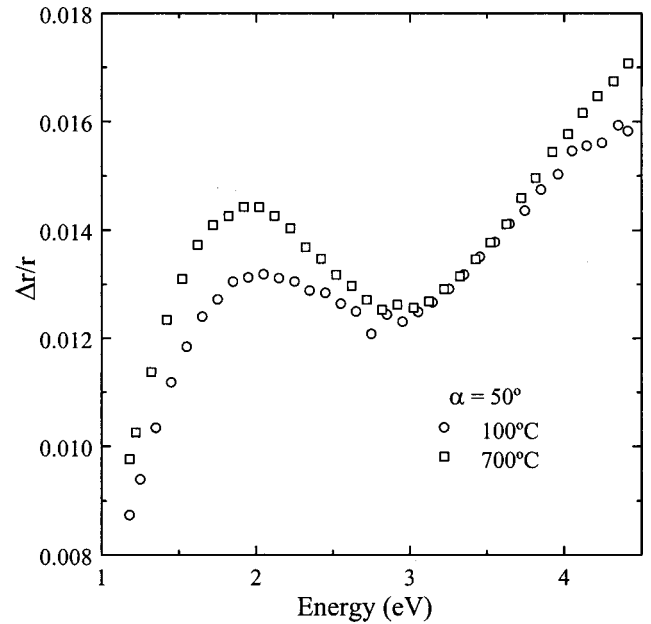

FIG. 3. Transverse Kerr spectra for selected LGT and HGT samples.

distorted and undistorted samples, as can be seen in the figures.

V. DISCUSSION

The first point to be clarified is the origin of the observed out-of-plane expansion in the Fe lattice. As already mentioned in Sec. III, there exists a large distortion in our Fe films that cannot be explained using elastic considerations. In order to elucidate the origin of this distortion, several test samples were grown at room temperature, under the same sputtering plasma conditions as those used for the samples shown in this paper, but with different capping layers. These
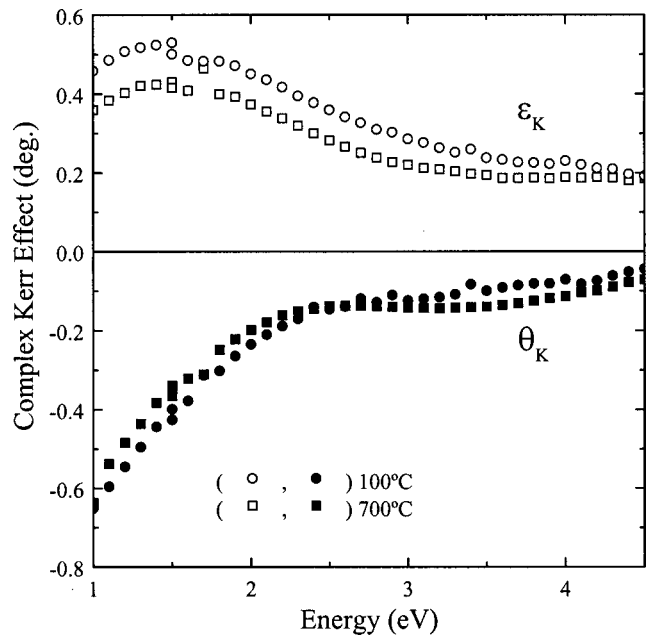

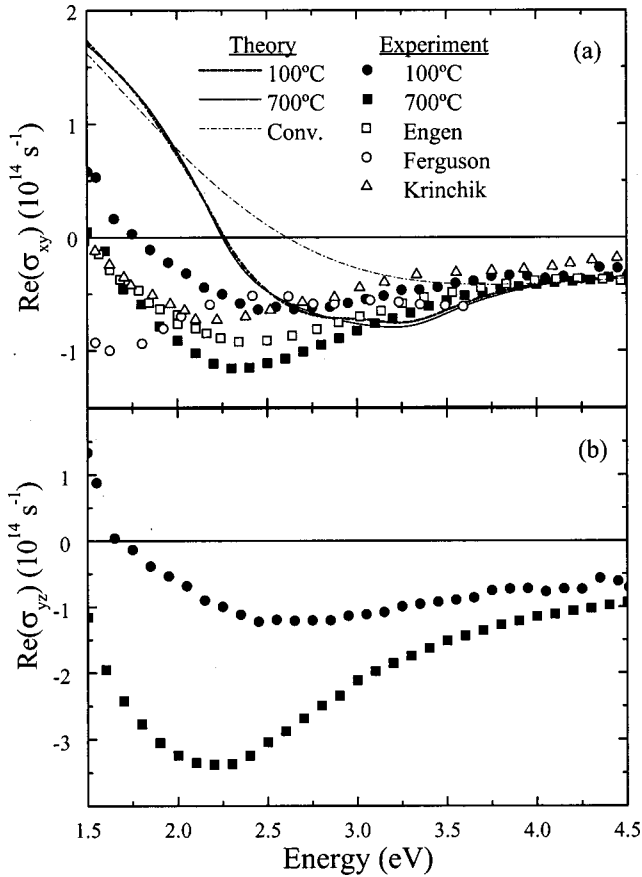FIG. 4. Complex Kerr effect measured for selected LGT and HGT samples.

FIG. 5. Real part of the off-diagonal elements of the conductivity tensor (a) σ_{xy} and (b) σ_{yz} for selected LGT and HGT samples. Theoretical results are also included for the case of $Re(\sigma_{xy})$ together with convolution (Conv.) with a Gaussian of full width at half maximum 1.5 eV for RT sample. Experimental results from Refs. 14, 15, and 27 are also shown.

FIG. 6. Imaginary part of the off-diagonal elements of the conductivity tensor (a) σ_{xy} and (b) σ_{yz} for selected LGT and HGT samples. Theoretical results are also included for the case of $Im(\sigma_{xy})$. Experimental results from Refs. 14, 15, and 27 are also shown.

test samples were capped with Pt (two samples) and Ti (one sample). One of the test samples capped with Pt was, prior to Pt deposition, exposed to reactive sputtering plasma identical to that used for the deposition of the TiN. A final sample was grown without capping and capped *ex situ* with wax immediately after its extraction from the deposition chamber to avoid oxidation as much as possible. Samples grown without any presence of N_2 showed expansions of 1.2% to 1.4% when capped *in situ* with Pt or Ti or *ex situ* with wax. On the other hand, samples exposed to N_2 for the reactive deposition of TiN or exposed to an $Ar+N_2$ plasma prior to the deposition of Pt presented expansions of 5.5% (see Table II for details). This clearly indicates that it is the presence of a reactive plasma and, in particular, the presence of nitrogen ions in the reactive plasma that induces the observed lattice distortions. In our interpretation, nitrogen penetrates into the Fe film through the crystallite grain boundaries. The amount of nitrogen entering the Fe film accounts for the lattice distortion. The density of grain boundaries increases with decreasing growth temperature (poorer structural quality as observed with RHEED). Thus nitrogen penetration is more effective for Fe films deposited at low temperatures (below 300 °C), yielding a higher distortion. The nitrogen penetration is more difficult in samples grown at high temperatures (over 300 °C), yielding a lower distortion. This fact explains
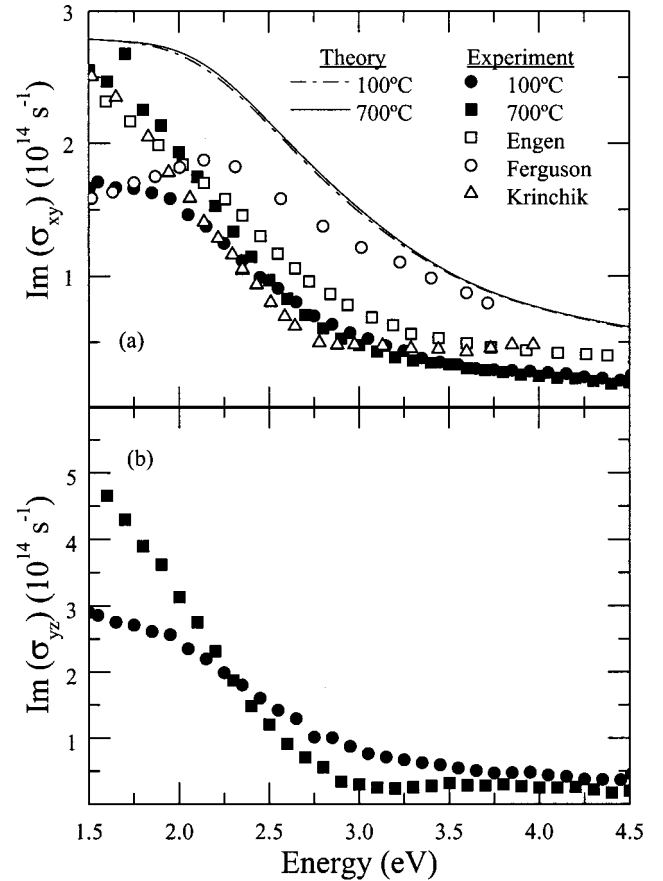
the differences in strain observed in our Fe films as a function of growth temperature. The influence of interstitial nitrogen on strain has been studied for Fe-N-Si sputter-deposited films,[28] where it was said to be the cause of a nonelastic component of the strain also. In our test samples there is still a nonelastic component of the strain, of the order of 1–1.5 %, that is not due to N. We propose to attribute this nonelastic component to residual strain that originates from interstitial Ar penetrating through grain boundaries in an analogous way to nitrogen. Since the size of an Ar atom is much larger than that of a N atom, the penetration of Ar into the Fe film will be lower too, explaining the observed reduced strain.

It is well known[29–31] that nitrogen reacts with Fe to form iron nitrides. Amongst these, the most similar ones to the structures we obtain correspond to $Fe_{16}N_2$, α'- and α''-martensite, with $a=2.86$ and 5.72 Å and $c=3.15$ and 6.29 Å, respectively. These phases have been prepared, for example, by reactive sputter deposition,[32] nitrogen ion implantation,[33] molecular-beam epitaxy in nitrogen ambient,[34] and ion-beam-assisted deposition.[35] The most similar deposition method to the one we have used is reactive sputtering. In all the reported works, the phase obtained immediately after reactive sputter deposition was α'-martensite. This indicates that in the present case we
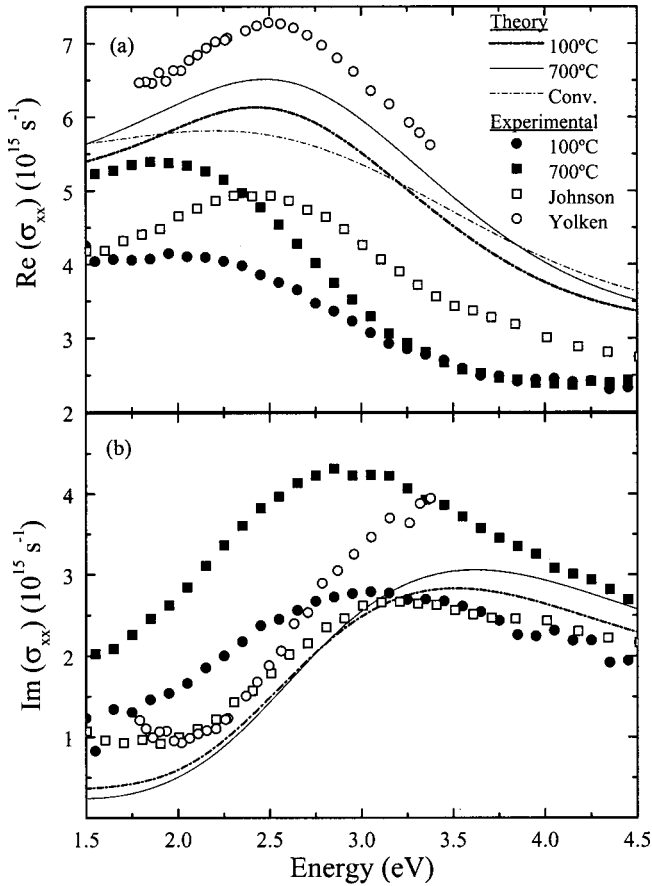
FIG. 7. Real (a) and imaginary (b) parts of the diagonal elements σ_{xx} of the conductivity tensor, experimental and theoretical results. Convolution (Conv.) with a Gaussian of full width at half maximum 1.5 eV for RT sample is included for Re(σ_{xx}). Experimental results from Refs. 12 and 13 are also shown.

should have an α'-like phase (lower order in the N positions). However, the out-of-plane lattice constant for the α' phase is 3.15 Å, a value much higher than that observed here (3.034 Å). This discrepancy excludes the possibility of formation of a pure α' phase. As the maximum strain observed here is approximately half that corresponding to (α',α'')-martensite, we conclude, by applying Vegard's law, that the maximum amount of nitrogen in our Fe films is approximately half that necessary to form α'- or

TABLE II. Perpendicular lattice parameters for test samples. Samples marked with an asterisk are those grown with no presence of N_2.

Capping	Out-of-plane lattice parameter (Å)	Out-of-plane expansion (%)
* Pt	2.905	1.4
Pt/(Ar+N$_2$ plasma)	3.021	5.4
* Ti	2.902	1.2
TiN	3.026	5.6
* Wax (*ex situ*)	2.905	1.4

α''-martensite. Consequently, we expect an atomic ratio of approximately 1N:16Fe, i.e., 6–7 % of N atoms, in our films. Given the amount of nitrogen found in the samples, we will attribute, in a first approach, the observed changes in the optical and magneto-optical spectra to lattice distortion, but not to the formation of a Fe_xN_y compound. Nevertheless, if the Fe grain boundaries are directional, offering preferential adsorption sites for nitrogen atoms, the different components of the conductivity tensor should be affected in different ways by this nitrogen. Transmission electron microscopy experiments might be useful in elucidating this question.

In order to investigate whether this N-induced deformation is sufficient by itself to explain the observed changes in the spectra, we have calculated the diagonal as well as the off-diagonal components of the conductivity tensor using the experimentally determined lattice parameters as input parameters in *ab initio* band-structure-based magneto-optical calculations. The results are presented in Figs. 5 [Re(σ_{xy},σ_{yz})], 6 [Im(σ_{xy},σ_{yz})], and 7 [Re(σ_{xx}),Im(σ_{xx})]. Our experimental and theoretical spectra show similar trends (lowering of the intensity of the transitions with increasing distortion), but they differ substantially in the magnitude of the changes.

Therefore, some other factors besides lattice distortion have to play an important role in the experimentally observed changes. Another possible factor that needs to be accounted for is the grain size, which is different for the sample grown at low temperature (85 Å) than for the sample grown at high temperature (120 Å). One way of taking this into account theoretically is to convolute the obtained spectra with a Gaussian whose width is related to the relaxation time. In Figs. 5(a) and 7(a) the influence of the relaxation time for Re(σ_{xx}) and Re(σ_{xy}) for a sample grown at RT is shown. In both cases, convoluting the theoretical calculations with a Gaussian leads to a broadening of the transition, a slight reduction in the intensity, and an increase in the difference between the relaxed and distorted calculated structures. Nevertheless, the convolution has a small influence on the energetic positions of the spectral features. In Fig. 7(a) [Re(σ_{xx})], this analysis shows that grain size could play some role, since the convoluted spectra are found to be closer to the experimental spectra than the nonconvoluted spectra. On the other hand, in Fig. 5(a), where Re(σ_{xy}) spectra are compared, the convoluted spectra differ more strongly from the experimental spectra than the nonconvoluted spectra. This suggests that the grain size can also affect the experimental results, but it is not sufficient to account for all the differences between the experimental and theoretical spectra.

Another possibility is hybridization between the nitrogen and iron orbitals, but this factor is not easy to take into account theoretically, without precise knowledge of the positions of the nitrogen atoms in the Fe lattice.

VI. CONCLUSIONS

Highly distorted Fe thin films (up to 6% expansion in the out-of-plane lattice parameter) can be obtained by incorporating N into the film through reactive deposition of a TiN capping layer. This N-induced distortion strongly depends on the Fe growth temperature, which determines grain size and therefore porosity of the film at the atomic scale. According

to Vegard's rule, the maximum amount of nitrogen expected in our Fe films is about 6–7 %. We consider this value as insufficient to form compounds such as α'- or α''-martensite.

No important differences are observed between different off-diagonal elements (σ_{xy} vs σ_{yz}) for a given tetragonally distorted sample. Stronger differences are found in these elements when comparing distorted vs relaxed samples. These differences are nevertheless smaller than in the diagonal elements.

The most important effects of the lattice distortion on the conductivity tensor occur in the diagonal terms, showing a decrease of the intensity and broadening of the peaks in the distorted samples with respect to the nondistorted ones. However, a comparison of the theoretical and experimental results shows that not only lattice distortion needs to be considered when a complete explanation of the observed effects is pursued. In this sense, other possible contributions have been proposed, such as differences in grain size and hybridization of the orbitals of nitrogen with those of iron.

*Corresponding author. FAX: 34 91 8060701, Email address: menendez@imm.cnm.csic.es

[1] B. Daudin, F. Widmann, G. Feuillet, Y. Samson, M. Arlery, and J. L. Rouvière, Phys. Rev. B **56**, R7069 (1997).

[2] J. Falta, D. Bahr, A. Hilla, G. Materlik, and H. J. Osten, Appl. Phys. Lett. **71**, 3525 (1997).

[3] J.-P. Locquet, J. Perret, J. Fompeyrine, E. Mächler, J. W. Seo, and G. Van Tendeloo, Nature (London) **394**, 453 (1998).

[4] *Strained Layers and Superlattices: Physics*, Vol. 32 of *Semiconductors and Semimetals*, edited by Thomas P. Pearsall (Academic, New York, 1990).

[5] M. Garfinkel, J. J. Tienmann, and W. E. Engeler, Phys. Rev. **148**, 695 (1966).

[6] D. K. Bagchi and B. D. Cullity, J. Appl. Phys. **38**, 999 (1967).

[7] B. D. Cullity, *Introduction to Magnetic Materials* (Addison-Wesley, Reading, Massachussetts, 1972).

[8] H. Kirchner, Ann. Phys. (Leipzig) **27**, 49 (1936).

[9] B. Lépine, C. Lallaizon, S. Ababou, A. Guivarc'h, S. Députier, A. Filipe, F. Nguyen Van Dau, A. Schuhl, F. Abel, and C. Cohen, J. Cryst. Growth **201/202**, 702 (1999).

[10] K. Nakajima, H. Sawada, T. Katayama, and T. Miyazaki, Phys. Rev. B **54**, 15 950 (1996).

[11] A. Delin, O. Eriksson, B. Johanson, S. Auluck, and J. M. Wills, Phys. Rev. B **60**, 14 105 (1999).

[12] P. B. Johnson and R. W. Christy, Phys. Rev. B **9**, 5056 (1974).

[13] H. T. Yolken and J. Kruger, J. Opt. Soc. Am. **55**, 842 (1965).

[14] G. S. Krinchik and V. A. Artemjev, J. Appl. Phys. **39**, 1276 (1968).

[15] P. E. Ferguson and R. J. Romagnoli, J. Appl. Phys. **40**, 1236 (1969).

[16] J. L. Erskine and E. A. Stern, Phys. Rev. Lett. **30**, 1329 (1973).

[17] P. M. Oppeneer, T. Maurer, J. Sticht, and J. Kübler, Phys. Rev. B **45**, 10 924 (1992).

[18] J. MacLaren and W. Huang, J. Appl. Phys. **79**, 6196 (1996).

[19] T. Gasche, M. S. S. Brooks, and B. Johanson, Phys. Rev. B **53**, 296 (1996).

[20] N. Mainkar, D. A. Browne, and J. Callaway, Phys. Rev. B **53**, 3692 (1996).

[21] J. H. Sexton, D. W. Lynch, R. L. Benbow, and N. V. Smith, Phys. Rev. B **37**, 2879 (1988).

[22] P. Hohenberg and W. Kohn, Phys. Rev. **136**, B864 (1964); W. Kohn and L. J. Sham, *ibid.* **140**, A1133 (1965).

[23] L. Hedin and B. I. Lundqvist, J. Phys. C **4**, 2064 (1971).

[24] O. K. Andersen, Phys. Rev. B **12**, 3060 (1975); H. L. Skriver, *The LMTO Method* (Springer, Berlin, 1984); J. M. Wills (unpublished); J. M. Wills and B. R. Cooper, Phys. Rev. B **36**, 3809 (1987); D. L. Price and B. R. Cooper, *ibid.* **39**, 4945 (1989).

[25] J. Zak, E. R. Moog, C. Liu, and S. D. Bader, J. Magn. Magn. Mater. **89**, 107 (1990).

[26] J. Zak, E. R. Moog, C. Liu, and S. D. Bader, Phys. Rev. B **43**, 6423 (1991).

[27] P. G. van Engen, Ph.D. thesis, Technical University Delft, 1983.

[28] K. Uchiyama and R. C. O'Handley, IEEE Trans. Magn. **35**, 2024 (1999).

[29] K. H. Jack, Proc. R. Soc. London, Ser. A **208**, 216 (1951).

[30] W. B. Pearson, *A Handbook of Lattice Spacings and Structures of Metals and Alloys* (MacMillan, New York, 1948).

[31] J. D. Fast and M. B. Verrijp, J. Iron Steel Inst., London **180**, 337 (1955).

[32] M. Takahashi, H. Shoji, H. Takahashi, H. Nashi, T. Wakiyama, M. Doi, and M. Matsui, J. Appl. Phys. **76**, 6642 (1994).

[33] K. Nakajima and S. Okamoto, Appl. Phys. Lett. **54**, 2536 (1989).

[34] Y. Sugita, H. Takahashi, M. Komuro, K. Mitsuoka, and A. Sakuma, J. Appl. Phys. **76**, 6637 (1994).

[35] Z.-Y. Zao, H. Jiang, Z.-K. Liu, D.-D. Huang, F.-G. Qin, S.-C. Zhu, and Y.-X. Sun, J. Magn. Magn. Mater. **177-181**, 1291 (1998).